International Multidimensional Engine Modeling User's Group Meeting, Detroit, MI, April 2020

Simulating the optical properties of soot using a stochastic soot model

T. Strickland*, S. Kokjohn
Department of Mechanical Engineering
University of Wisconsin - Madison
Madison, WI 53706 USA

Abstract

KL extinction measurements are common in literature concerning soot producing sprays because of their non-intrusiveness. Unfortunately, these measurements often rely on bold assumptions of uniform and monodisperse spherical particles. In this work, a Spray A case is simulated using a highly detailed 3D stochastic soot model and the measured and simulated soot volume fraction are compared. Although the simulated volume fraction magnitude is approximately correct, features are much sharper than in the measured data. Optical models based on particle shape are applied to the simulated soot particles to find the local optical thickness. The modeled optical thickness aligns with the measured volume fraction much more closely than the simulated volume fraction indicating KL extinction measurements are not simply related to soot volume fraction.

*Corresponding Author: testrickland@wisc.edu

1 Introduction

Ferin et al. [1] has shown that soot like particles on the order of 10nm in diameter are potentially damaging to pulmonary alveoli tissue of the lungs. Such particles are small enough to bypass the functional filtering organs while large enough to not be easily lavaged by biokinetic processes. In response to these health and additional aerosol and environmental concerns, regulations on soot are progressively becoming more stringent. This includes recently imposed soot particle size concerned additions to regulations [2]. To meet these regulations an increased fundamental understanding of soot is required.

The scientific method for developing an understanding consists of creating a theory based on observations and then confirming the theory with further observations/measurements. Spray A is a standardized test to produces these observations. Spray A is designed to exhibit real-world diesel combustion phenomenon, while providing visual access to the jet for soot measurements via KL extinction. Although KL extinction provides one of the best ways to non-intrusively sample soot, assumptions on the uniformity of soot may not hold under all conditions. In the work of Skeen et al.[3], two light sources with different wavelengths were used to measure the optical thickness of soot. Then the differences between the calculated values were analyzed as an indicator of nonuniform optical soot properties. The variability in optical properties reduces the accuracy and usefulness of KL extinction measurements for soot, regulating them to qualitative observations [4]. Theory often outpaces measurement capability, but simulation, a virtual experiment based on theory, can be used as a stopgap between theory and experimentation [5]. With this motivation, the importance of particle shape in KL extinction methods will be investigated using simulations.

Theory

Light extinction measurements are used to quantify the concentration of an opaque substance along a path. The transmittance,

$$\frac{I}{I_0} = \exp\left(-K_e L\right), \tag{1}$$

where $\frac{I}{I_0}$ is the ratio of collected light intensity with and without soot, gives the optical thickness, $-K_e L$, of the volume that the light passes through.

More generally, if the volume the light traverses is not uniform,

$$K_e L = \int_{Z_{-\inf}}^{Z_{\inf}} K_e dz. \tag{2}$$

The extinction coefficient, K_e, is given as a sum over the particles in the path,

$$K_e = \sum_{i=1}^{\frac{M0}{\Omega}} \sigma_i^2 \pi Q_{ei} dr \tag{3}$$

where σ is the optical attenuation radius, Ω is a differential volume, $M0$ is the particle concentration in that volume, and the extinction efficiency is the sum of the scattering, Q_s, and absorption, Q_a, efficiency,

$$Q_e = Q_s + Q_a \tag{4}$$

[6].

Small particle Mie theory gives models for Q_s and Q_a of a single particle assuming the particle is spherical. For particles in the Rayleigh limit, where

$$x_p = \frac{\pi\sigma}{\lambda} \tag{5}$$

is less than 1, Q_a can be approximated by

$$Q_a = 4 x_p E(m) \tag{6}$$

where

$$E(m) = \Im\left(\frac{m^2-1}{m^2+2}\right). \tag{7}$$

Q_s can be approximated by

$$Q_s = \frac{8}{3} x_p^4 F(m) \tag{8}$$

where

$$F(m) = \left|\frac{m^2-1}{m^2+2}\right|^2. \tag{9}$$

If the domain is further assumed to be monodisperse then the total expression for K_e collapses to

$$K_e = f_v \frac{6\pi}{\lambda}(1+\alpha_{sa})E(m), \tag{10}$$

where α_{sa} is the scattering to absorption ratio and f_v is the volume fraction. In extinction measurements reproducing the soot volume fraction field, as in Fig. 2a, it is typical to use this relation with an empirically determined constant value of $(1+\alpha_{sa})E(m) = 0.46$ [7] due to a lack of alternative soot information, despite studies [8] showing soot particles spanning a wide array of not only size but also form, throughout a combustion event. Other literature [9, 6] assumes a zeroth-order log-normal distribution of soot particle sizes in a polydisperse volume to create a relation requiring soot population moments. Rayleigh-Debye-Gans theory gives the scattering efficiency for a porous sphere as

$$Q_s^{'} = Q_s Y_a. \tag{11}$$

The porous sphere has been adopted to soot by Dobbins et al. [10] using a model for Y_a

$$Y_a = k_f \left(\frac{3D_f}{16x_p} \right)^{D_f/2} \tag{12}$$

An empirical correction of the extinction efficiency given by Mackowski et al. [11],

$$Q_e^{'} = Q_s + log(n_p)Q_a, \tag{13}$$

accounts for the aggregate nature of a soot particle. In this work, assumptions will be made when lacking the requisite information to use an applicable model, such is the case for the refractive index of soot, or when the available information is not exactly the value required, such as the attenuation diameter. Soot particle bound and free electron densities used for refractive index models, such as the Drude-Lorentz dispersion model, are not immediately provided by the soot model used so the literature prevalent constant refractive index of $1.57 + 0.56i$ will be used for soot. Zhang et al. [6] collected data from multiple studies to find a refractive index of $1.57 + 0.56i$ an average soot value. The attenuation diameter was given by the soot chemistry collision diameter due to their similar purpose of representing the likelihood of getting in the way of particles or light.

Case Setup

Spray A is an industry standard diesel like injection into a constant volume domain that provides visual access. For this particular iteration of Spray A, Dodecane is injected at 1500 bar for 4 ms into 15 percent oxygen, 1000K ambient conditions resulting in a pseudo-steady state duration from 2.5 to 4.0 ms after the start of injection. Measured results used in this study are from Skeen et al. [3] except for OH images, due to availability. OH images are from Abraham et al. [12]. Despite not having the images of Skeen et al., the lift of length was published as 11.5mm which is very close to 12.2mm, reported by Abraham et al.. Both of the experiments use the same spray A conditions summarized in Table 1.

The case is simulated using an in-house computational fluid dynamics (CFD) code based on the KIVA family of codes [14]. The code includes improved physical models developed at the University of Wisconsin-Madison's Engine Research Center (ERC). The spray model uses the Lagrangian-Drop and Eulerian-Fluid (LDEF) approach. To reduce the grid size dependency of the LDEF spray model and allow accurate spray simulation on a relatively coarse grid, the Gasjet model of Abani et al. [15]

$T_{ambient}$	1000 K
$\rho_{ambient}$	22.8 kg/m^3
$O_2, ambient$	15 %
Fuel	c12h26
Inj. Duration	4 ms
Nozzle	90 μm
Injection Pressure	1500 bar
Pseudo-steady	2.5-4.0 ms
Laser	HeNe

Table 1: Spray A experimental conditions

Simulation package	KIVA3v Rev 2
Soot model	Direct
Turbulent model	RANS (RNG k-ϵ)
Reaction Mech.	Multi component w/ PAH [13]
Fuel	$C_{12}H_{26}$
Mesh	Pseudo 2D
Base mesh (mm)	1.0

Table 2: Spray A simulation parameters

is used to model the relative velocity between the droplets and gas phase in the near nozzle region. The Kelvin Helmholtz- Rayleigh Taylor (KH-RT) model was used to model the spray breakup [16]. The Re-Normalization Group (RNG) k- model was used for turbulent flow calculation [17]. The chemistry calculations were performed by SpeedChem, a sparse analytical jacobian solver coupled to the CFD [18]. The Multicomponent wide distillate mechanism developed by Ren et al. [13] was the chosen chemical mechanism due to its reasonable size and PAH pathway. The mechanism consists of 178 species and 758 reactions including a PAH pathway that extends to benzopyrene, the subsequent PAH after pyrene. A mesh size with a characteristic dimension of 1 mm was selected by performing a grid sensitivity study. It was found that this grid size gave an acceptable trade-off between accuracy and computational expense.

Soot is modeled using a fully coupled Lagrangian parcel - Eulerian fluid implementation of a highly detailed stochastic soot model based on SWEEP. SWEEP is a modified Monte-Carlo method soot model developed by or including the works of Balthasar et al. [19], Celnik et al. [20] and Patterson et al. [21] and distributed by Cambridge CoMo group. The modifications to SWEEP include a majorant kernel developed Goodson et al. [22]to replace the coagulation kernel and linear process deferment

algorithm (LDPA) developed by Patterson et al. [23] to increase the numerical speed. The Lagrangian - Eulerian coupling relies on creating a partition over the simulated domain of pseudo-homogeneous subdomains to support individual stochastic soot model instances. The model is highly phenomenological and has no explicit tuning parameters. Further details can be found in [24]. The simulation parameters are listed in Table 2.

The current CFD approach has been applied to a range of spray and engine combustion cases using a variety of fuels; accordingly, only validation relevant to the present work is presented here. Further validation can be found in references [25, 24]. Soot is a product of incomplete combustion so accurate soot predictions rely on the entire simulation scope including mixing, gas chemistry, and finally soot production [26]. As such, the combustion simulations need to be validated.

Lift-off length is a common measure of simulation accuracy since it involves mixing and combustion. Fig. 1 shows a comparison between the measured OH chemiluminescence and simulated OH mole fraction under pseudo steady conditions. In the figure, the injector is out of view on the left. The upper half is the simulated OH concentration across the centerplane at 4ms and the lower half is the ensemble averaged measured OH chemiluminescence. Both images are to scale and span the same domain. The overall jet structure is captured by the simulation well; however, the lift-off length is over predicted by approximately 3 mm. This agreement is similar to other studies (e.g., [27]) and is deemed acceptable.

Using KL extinction methods, volume fraction measurements were taken during quasi steady state, after the spray head leaves the viewing window and until the end of injection, beginning at 2.5ms and going until 4.0ms. More details on the measurement methods are given in [3].

Fig. 2 shows surfaces, colored by the corresponding scale for the indicated value. The injector tip is out of view in the lower left-hand corner at $(0, 0)$. The surfaces represent the right half of the axisymmetric central plane of the jet with time averaged values over the pseudo steady state range. Figs. 2a and 2b compare the measured and simulated volume fraction. The simulated volume fraction has much steeper gradients than the measured results, however, both share some distinctive features. Both have wings preceding the main sooty body where there is a higher volume fraction in the perimeter than in the core. The measured wings are much softer and end much sooner than the simulated wings. In general, the simulated sooty volume fraction body seems to be shifted further away from the injector nozzle and most of the sooty region's core near the axis seems to be missing. Magnitude wise the simulated and measured volume fraction are in very good agreement, especially for soot results. As stated earlier, the measured results are based on soot with constant optical properties. The following is an investigation into the validity of that assumption.

Analysis

Particle Size Distributions

Fig. 4 shows a collection of local PSDs over the entire Spray A domain. Particles are sized according to their electrodynamic diameter. The number of the plot corresponds to the PSDs axial location and the color of the PSD corresponds to is radial location. The bold black PSD is the cumulative radial PSD for that plot's corresponding axial location. The map to interpret the location of the PSD is in Fig. 3. Fig. 3 is a surface of spray A colored by the modeled extinction coefficient. The color legend, however, corresponds to the radial distance from the jet centerline. The PSD colors of Fig. 4 follow the same radial location legend. The zones corresponding to the plots of Fig. 4 are also numbered in Fig. 3.

Soot evolution in the jet as it is transported downstream is easily visible in Fig. 4. The progression from inception at roughly 2.5cm (Fig. 4.3) to mature soot, 5cm (Fig. 4.9), and finally into decay, 6.5cm (Fig. 4.13), can be identified by moving axially away from the injector.

Moving radially away from the injection axis shows different patterns depending on the axial location. 3cm (Fig. 4.5) downstream from the nozzle, the largest particles are found in an annular region, bounded internally and externally by smaller particles. At approximately 4cm (4.7) the largest particles are represented at the perimeter of the sooty region and smaller near the axis. Finally, at approximately 5.25cm (4.10) all radial locations exhibit some fully mature particles, however, there is still a slight radial gradient from the smallest to largest particles. Going further downstream, PSDs collapse as the sooty region narrows to a point. Beyond 5.25cm, perimeter PSDs exhibit the most diversity in mature and medium sized particles while central PSDs are typically more concentrated at a single largest mode. It is clear that although the section averaged PSDs (Black curves of Fig. 4) maintain a relatively similar shape over much of the domain, bimodal with a maximum diameter of about $100nm$, the constitution of said PSDs varies greatly.

Based on the complex variability of PSDs with respect to location, the relation between particle size and particle type is worth investigation.

Particle Form

Fig. 5 shows surface plots in a similar format to Fig. 2, however Fig. 5a is colored by the average particle optical attenuation diameter, Fig. 5b is colored by the average number of primary particles per soot agglomerate, Fig. 5c is colored by the average particle extinction efficiency, $Q_e^{'}$ from Eq. 13, and Fig. 5d is colored by the number of soot particles per volume, $M0$ from Eq. 3.

Figs. 5a and 5b are both plots indicating the average soot particle type in a given region. Fig. 5a shows that in the body of the sooty region, particles at the core have a smaller attenuation diameter than the surrounding particles despite having roughly the same electrostatic diameter as shown in Fig. 4.10. Fig. 5b provides some explanation, showing particles nearer to the core having more primary particles on average, effectively lowering their fractal dimension and making the particle less compact. The same relation is visible at the head of the sooty region (i.e., along the axis). As the particles move into the oxidizing region, they trade compactness for primary particles. These figures continue to show that the particle population is not uniform and the prevalent particle types are a strong function of location. Due to this variability and attenuation's reliance on particles' form, the investigation continues to a model for the optical extinction coefficient based on particle shape.

Particle Optics

Figs. 5c and 5d along with Fig. 5a show the average contributing terms to Eq. 3 as a function of location. Fig. 5d shows that the number of soot particles is maximized much closer to the injector nozzle than areas of considerable volume fraction seen in Fig. 2. The number of particles is inversely related to the extinction efficiency at approximately 5cm away from the injector nozzle where substantial particle growth occurs by coagulation. The extinction efficiency of Fig. 5c finds its shape as a combination of the patterns seen in figures 5a and 5b. Attenuation diameter's influence is found in Eqs. 6 and 11 via x_p and the strong core is a function of the less compact soot particles that exhibit increased scattering efficiency seen in Eq. 12. The extinction efficiency also shares a similar shape to the volume fraction.

Coefficient of Extinction

Equation 10 is solved over the whole domain by iterating through all of the stochastic soot particles and solving for each particle's contribution. Fig. 2d shows the resulting surface plot colored by K_e. For comparison,

$$K_e = f_v \frac{6\pi}{\lambda}(1 + \alpha_{sa})E(m), \tag{14}$$

where $(1+\alpha_{sa})E(m) = 0.46$, is solved using the simulated volume fraction and plotted in Fig. 2c Note that the right side is simply a scaled soot volume fraction plot and that it makes the same assumptions that the measured data of plot 2a make.

Fig. 2d shows that the opacity of soot is not related proportionally to the volume fraction of soot. Specifically, regions of high opacity are expanded to the core and extend further to the perimeter of the sooty region. Looking at Fig. 2a, the measured data exhibit these exact properties with respect to the simulated volume fraction results. The simulated results still deviate from the exact form of the measured results by having sharper wings and high attenuation surrounding the core where the measured results have a much softer gradient that monotonically reaches a maximum attenuation at the core. Comparing the magnitudes of figures 2d and 2c shows that the measurements are generally under-predicting the soot despite the volume fraction plots of Fig. 2a and 2b being approximately correct magnitude wise. Possible sources for the remaining error include soot particle motion deviation from the bulk Eulerian fluid motion, inaccurate soot surface chemistry, and unaccounted variability of soot optical properties, such as refractive index, or inaccurate models for scattering efficiency of a highly diverse soot population.

Conclusion

A soot simulation using a detailed stochastic soot model was used to simulate a Spray A case. The combustion simulation was validated by comparing the liftoff length, however, the experimental soot volume fraction, measured using KL extinction and assuming a monodisperse spherical soot population, and simulated soot volume fraction showed substantial differences. The simulated soot volume fraction gradients were sharper and had its region of maximum soot volume fraction away from the axis. Using models for attenuation, absorption, and scattering the optical extinction coefficient was found for the simulated soot. This modeled field was compared to the field of extinction coefficient created using the constant soot optical properties

assumed in the measurements. The modeled extinction coefficient revealed a profile that matched the measured profile much more closely with much more absorption near the axis. Even allowing the possibility of relatively inaccurate soot simulation, these results indicate that local soot particle shape is an important factor in KL extinction measurements for soot volume fraction.

Nomenclature

Variables

D_f	fractal dimension
E	optical property
F	optical property
f_v	soot volume fraction
K	optical coefficient
L	optical path length
m	complex index of refraction
$M0$	soot particle concentration
n_p	number of primary particles in a soot aggregate
Q	optical efficiency
x_p	dimensionless particle size
Y_a	scattering correction coefficient

Operators

$'$	corrected

Subscripts

a	absorption
e	extinction
s	total scattering

Greek Symbols

α_{sa}	scattering to absorption ratio
λ	wavelength
Ω	differential volume
σ	attenuation radius

References

[1] JURAJ FERIN, GÜNTER OBERDÖRSTER, SIDNEY C SODERHOLM, and ROBERT GELEIN. *Journal of aerosol medicine*, 4(1):57–68, 1991.

[2] PEAN UNION. Regulation (ec) no 715/2007 of the european parliament and of the council. Technical report, 715/2007/EC, 2007.

[3] Scott A Skeen, Julien Manin, Kristine Dalen, and Lyle M Pickett. *8th US National combustion meeting*, 2013.

[4] Sanghoon Kook and Lyle M. Pickett. 5:647–664, 01 2012.

[5] Role of modeling and simulation in scientific discovery, Jan 2013.

[6] Q. Zhang and P.A. Rubini. *Fire Safety Journal*, 46(3):96 – 103, 2011.

[7] Julien Manin, Lyle M Pickett, and Scott A Skeen. *SAE International Journal of Engines*, 6(4):1908–1921, 2013.

[8] Jill M. Williams and Louis A. Gritzo. *Symposium (International) on Combustion*, 27(2):2707 – 2714, 1998.

[9] Hsueh-chia Chang and T. T. Charalampopoulos. *Proceedings of the Royal Society of London. Series A: Mathematical and Physical Sciences*, 430(1880):577–591, 1990.

[10] Richard A. Dobbins and Constantine M. Megaridis. *Appl. Opt.*, 30(33):4747–4754, Nov 1991.

[11] Daniel W. Mackowski. *Appl. Opt.*, 34(18):3535, June 1995.

[12] Lyle M. Pickett and John P. Abraham. *Atomization and Sprays*, 20(3):241–250, 2010.

[13] Shuojin Ren, Sage L Kokjohn, Zhi Wang, Haoye Liu, Buyu Wang, and Jianxin Wang. *Fuel*, 208:447–468, 2017.

[14] Y Ra and RD Reitz. *International Journal of Engine Research*, 4(3):193–218, 2003.

[15] Neerav Abani and Rolf D Reitz. *ILASS Americas, 20th Annual Conference on Liquid Atomization and Spray Systems*, 2007.

[16] Jennifer C. Beale and Rolf D. Reitz. *Atomization and Sprays*, 9(6):623–650, 1999.

[17] Zhiyu Han and Rolf D Reitz. *Combustion science and technology*, 106(4-6):267–295, 1995.

[18] Federico Perini, Emanuele Galligani, and Rolf D. Reitz. *Energy & Fuels*, 26(8):4804–4822, 2012.

[19] M Balthasar and M Kraft. *Combustion and Flame*, 133(3):289 – 298, 2003.

[20] Matthew Celnik, Robert Patterson, Markus Kraft, and Wolfgang Wagner. *Combustion and Flame*, 148(3):158 – 176, 2007.

[21] Robert IA Patterson, Jasdeep Singh, Michael Balthasar, Markus Kraft, and Wolfgang Wagner. *Combustion and Flame*, 145(3):638–642, 2006. developes harmonic mean coagulation kernel formulation.

[22] Michael Goodson and Markus Kraft. *Journal of Computational Physics*, 183(1):210 – 232, 2002.

[23] R. I. A. Patterson, J. Singh, M. Balthasar, M. Kraft, and J. R. Norris. *SIAM Journal on Scientific Computing*, 28(1):303–320, 2006.

[24] Tyler Strickland and Sage Kokjohn. *2018 Spring Technical Meeting, Central States Section of The Combustion Institute*, 2018.

[25] Flavio D. F. Chuahy. PhD thesis, University of Wisconsin, Madison, 2018. Copyright - Database copyright ProQuest LLC; ProQuest does not claim copyright in the individual underlying works; Last updated - 2019-10-18.

[26] H. Bockhorn. *Soot Formation in Combustion: Mechanisms and Models*. Springer Series in Chemical Physics. Springer Berlin Heidelberg, 2013.

[27] Sibendu Som, Douglas E Longman, Zhaoyu Luo, Max Plomer, Tianfeng Lu, Peter K Senecal, and Eric Pomraning. *Journal of Energy Resources Technology*, 134(3):032204, 2012.

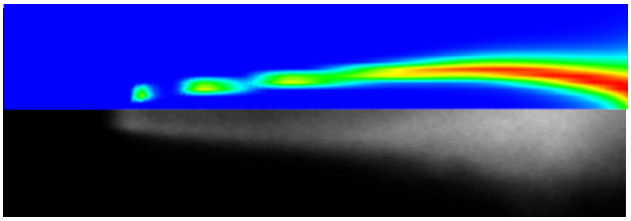

Figure 1: Spray A steady state lift off length (upper) simulated OH concentration (lower) measured OH chemoluminescence of Abraham et al. [12]. The image domain is 7.0cm long and 2.3cm wide.

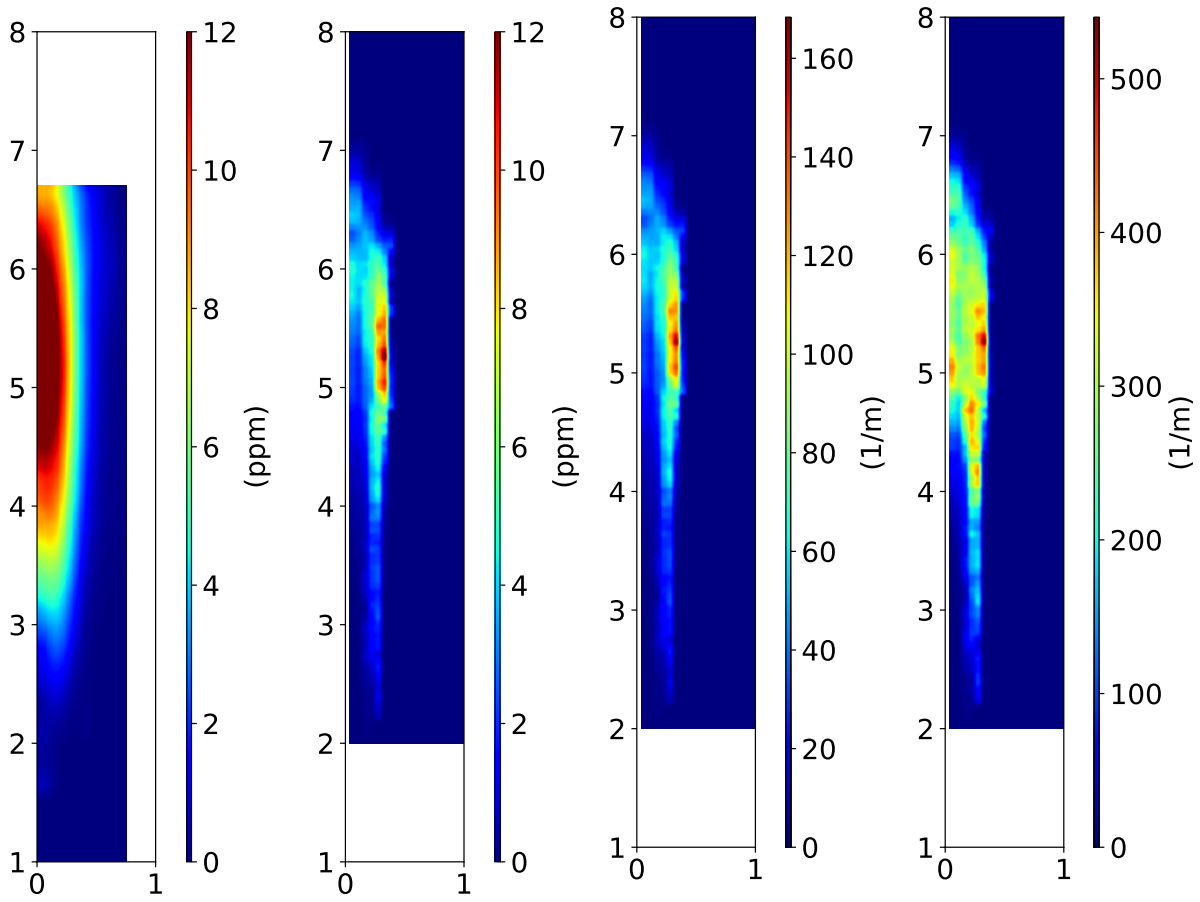

(a) measured volume fraction

(b) simulated volume fraction

(c) average extinction coefficient calculated using soot particle concentration

(d) average extinction coefficient calculated using Eq. 3

Figure 2: Surface plots of the time averaged indicated value. Surfaces are bisections of the central axial plane.

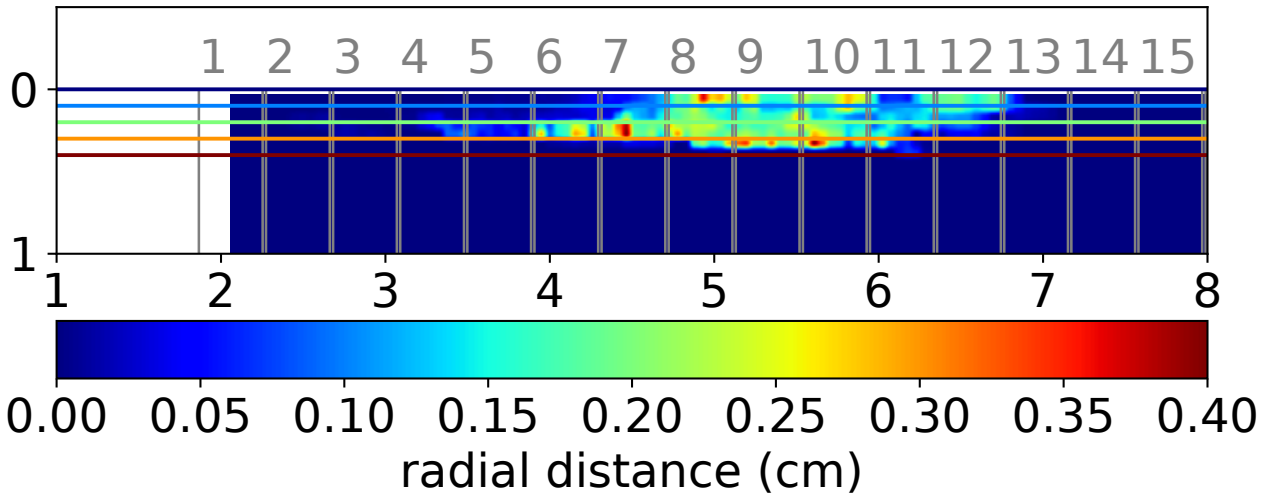

Figure 3: Map of locations for PSDs in Fig. 4. Numbered box corresponds to plot number and colorbar corresponds to radial distance. For example, the orange PSD curve in Fig. 4.10, was constructed from the soot at an axial distance of approximately 5.25 cm and a radial distance of 0.3 cm.

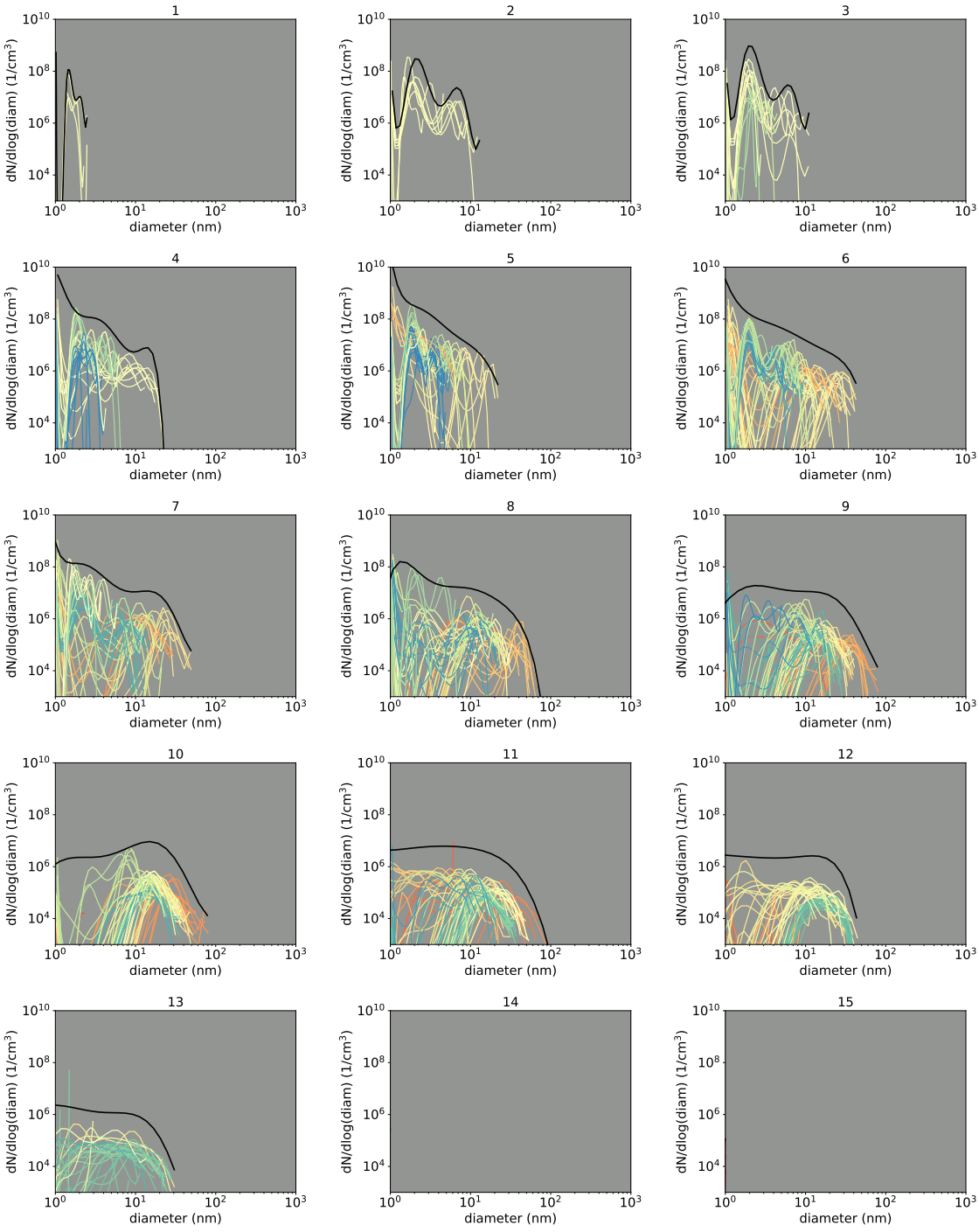

Figure 4: PSDs across all soot producing regions of the domain at 5 ms after the start of injection. Each colored curve represents a cell sized region (1cm characteristic length). Each black curve represents the axial section cumulative. Refer to Fig. 3 for an explanation of location interpretation. Diameter is electrodynamic diameter.

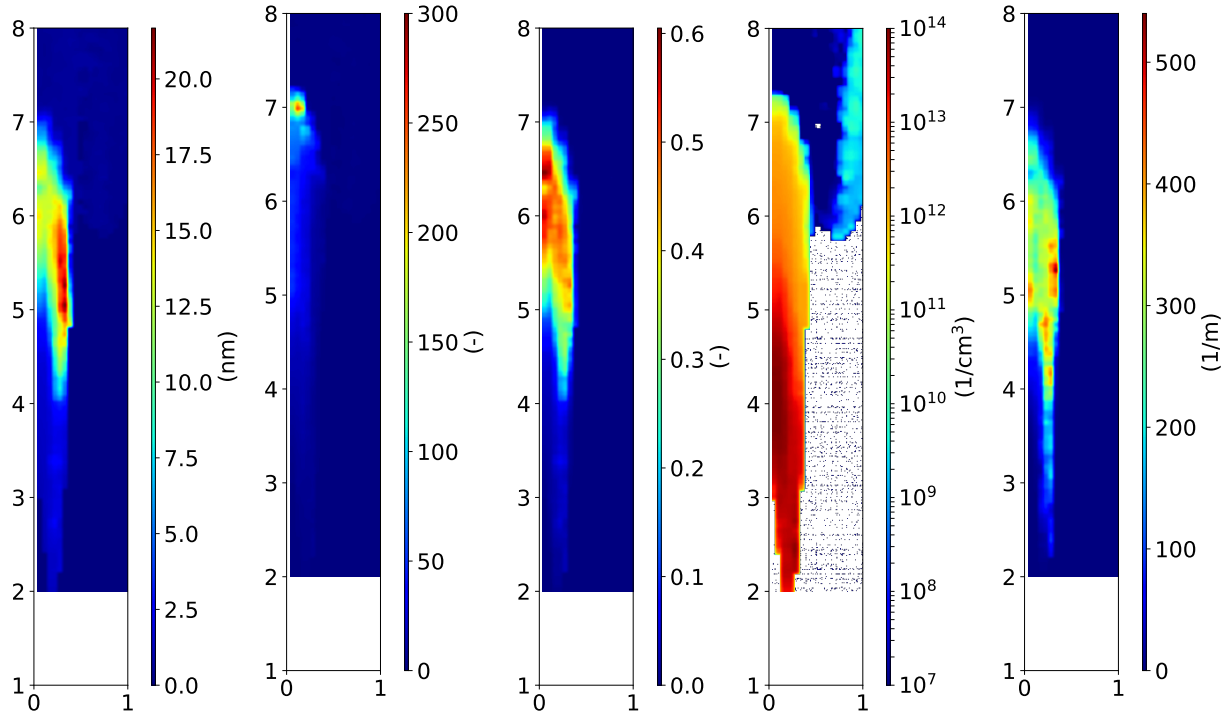

(a) average attenuation radius

(b) average number of primary particles per agglomerate

(c) average extinction efficiency

(d) soot particle concentration

(e) average extinction coefficient calculated using Eq. 3

Figure 5: Surface plots of the time averaged indicated value. Surfaces are bisections of the central axial plane.